Nanoscale

PAPER

View Article Online
View Journal | View Issue

Cite this: *Nanoscale*, 2017, **9**, 10404

Overcoming multidrug resistance using folate receptor-targeted and pH-responsive polymeric nanogels containing covalently entrapped doxorubicin†

Y. Chen,‡[a] O. Tezcan,‡[b] D. Li,[a] N. Beztsinna,[a] B. Lou,[a] T. Etrych,[c] K. Ulbrich,[c] J. M. Metselaar,[b,d] T. Lammers[a,b,d] and W. E. Hennink*[a]

Multidrug resistance (MDR) contributes to failure of chemotherapy. We here show that biodegradable polymeric nanogels are able to overcome MDR *via* folic acid targeting. The nanogels are based on hydroxyethyl methacrylamide-oligoglycolates-derivatized poly(hydroxyethyl methacrylamide-*co*-*N*-(2-azidoethyl)methacrylamide) (p(HEMAm-*co*-AzEMAm)-Gly-HEMAm), covalently loaded with the chemotherapeutic drug doxorubicin (DOX) and subsequently decorated with a folic acid-PEG conjugate *via* copper-free click chemistry. pH-Responsive drug release is achieved *via* the acid-labile hydrazone bond between DOX and the methacrylamide polymeric network. Cellular uptake and cytotoxicity analyses in folate receptor-positive B16F10 melanoma *versus* folate receptor-negative A549 lung carcinoma cells confirmed specific uptake of the targeted nanogels. Confocal microscopy demonstrated efficient internalization, lysosomal trafficking, drug release and nuclear localization of DOX. We also show that DOX resistance in 4T1 breast cancer cells results in upregulation of the folate receptor, and that folic acid targeted nanogels can be employed to bypass drug efflux pumps, resulting in highly efficient killing of resistant cancer cells. In conclusion, folic acid functionalized nanogels with pH-controlled drug release seem to hold significant potential for treating multidrug resistant malignancies.

Received 19th May 2017,
Accepted 30th June 2017

DOI: 10.1039/c7nr03592f

rsc.li/nanoscale

1 Introduction

Chemotherapy is extensively used to treat cancer.[1] Chemotherapeutic drugs, however, suffer from several drawbacks, including poor pharmacokinetics, low tumor accumulation and significant off-target localization, together resulting in suboptimal efficacy and high toxicity.[2–4]

An additional issue complicating chemotherapy is multidrug resistance (MDR).[5] MDR can exist intrinsically, but generally gradually develops during the chemotherapeutic treatment of initially sensitive cells.[6] Multiple mechanisms contribute to MDR, including inhibition of drug-induced apoptosis, activation of DNA damage repair mechanisms, and increased expression of drug efflux pumps.[7,8] These efflux pumps recognize a broad range of drug molecules, and rapidly and efficiently transport low molecular weight chemotherapeutic agents out of cancer cells.

One of the strategies to overcome MDR is to use nanomedicine-based drug delivery systems.[9] Because of their much larger size, nanomedicines are internalized *via* endocytosis[10–12] instead of passive diffusion across the cell membrane, thereby bypassing the drug efflux pumps responsible for MDR.

Nanogels have emerged as a promising platform for drug delivery because of their high loading capacity, good biocompatibility and biodegradability.[13,14] Nanogels are stable submicrometer hydrogels consisting of crosslinked swollen hydrophilic polymer networks with high water content (>95%).[15] By varying the chemical composition of nanogels, their characteristics such as size, charge, porosity, softness and degradability can be fine-tuned and tailored. By introducing stimuli-sensitive groups between payloads and nanogel networks,

[a]*Department of Pharmaceutics, Utrecht Institute for Pharmaceutical Sciences, Utrecht University, Utrecht, 3584 CG, The Netherlands. E-mail: W.E.Hennink@uu.nl*
[b]*Department of Nanomedicine and Theranostics, Institute for Experimental Molecular Imaging, RWTH Aachen University Clinic, 52074 Aachen, Germany*
[c]*Institute of Macromolecular Chemistry, Czech Academy of Sciences, Heyrovsky Square 2, 162 06 Prague 6, Czech Republic*
[d]*Department of Targeted Therapeutics, MIRA Institute for Biomedical Engineering and Technical Medicine, University of Twente, Enschede, 7522 NB, The Netherlands*
† Electronic supplementary information (ESI) available: Synthesis and characterization of monomers and polymers, uptake kinetics of free DOX in B16F10 cells, Pgp expression in the resistant cells, and IC50 of different formulations incubated with different cell lines. See DOI: 10.1039/c7nr03592f
‡ These authors contributed equally to this work.

controlled release at the target site can be achieved because of the difference in physiological environment between normal and pathological tissues.[16–18]

Nanogels, like other nanomedicine formulations, can be surface-modified with ligands to enable active targeting.[19,20] Ligand-modified nanoparticles recognize and bind to their target *via* specific ligand–receptor interactions. In case of MDR, the chondroitin sulfate proteoglycan CD44 (which binds to hyaluronic acid, HA) has recently emerged as an interesting target.[21] Also certain integrins, which can *e.g.* be recognized by RGD peptides, may be useful for targeting multidrug resistant cells and tumors.[22]

The folate receptor (FR) is upregulated in many types of cancer cells and has been extensively used as a target in nanomedicine-mediated drug delivery.[23] Not much is known, however, about the regulation and role of FR in MDR cancers. In 4T1 breast cancer cells continuously exposed to gradually increasing concentrations of doxorubicin (DOX), we tested FR regulation and we set out to develop folic acid targeted nanogels for more efficient treatment of MDR cancers.

To this end, we prepared biodegradable p(HEMAm-*co*-AzEMAm)-Gly-HEMAm-based polymeric nanogels containing methacrylamided doxorubicin derivatives conjugated to the nanogel backbone *via* pH-sensitive hydrazone linkages (Fig. 1). The surface of nanogels was modified with polyethylene glycol (PEG) and FA-PEG *via* copper-free click chemistry to enable targeting of FR-expressing MDR cancer cells (Fig. 2).

2 Experimental

2.1 Materials

N-(2-Hydroxyethyl)methacrylamide (HEMAm) and HEMAm-oligoglycolates (HEMAm-Gly) with degree of polymerization of 1.8 were synthesized as previously described.[24–26] DOX methacrylamide-based derivative (DOX-MA, 6-methacrylamidohexanoylhydrazide-DOX, with DOX·HCl content 75 wt%) was synthesized as described previously.[27] DOX·HCl (purity ≥98%) was purchased from Guanyu bio-technology Co., Ltd (Xi'an, China). BCN-PEG$_{5000}$-OMe (purity ≥90%) was purchased from SynAffix BV (Oss, the Netherlands). Boc protected amine PEG amine (Boc-NH-PEG-NH$_2$, M_w 5000 kDa) was purchased from Creative PEGWorks (Chapel Hill, USA). Irgacure 2959 was obtained from Ciba Specialty Chemicals Inc. (Hercules, USA). ABIL EM 90 was provided from Evonik Industries AG (Essen, Germany). Folic acid (purity ≥97%) was purchased from Sigma-Aldrich (Zwijndrecht, the Netherlands). Acetonitrile (ACN, HPLC grade), dichloromethane (DCM, peptide synthesis grade), dimethylformamide (DMF, peptide synthesis grade), ethyl acetate (AR grade), methanol (HPLC grade), hexane (HPLC grade) and dimethyl sulfoxide (DMSO, AR grade) were obtained from Biosolve (Valkenswaard, the Netherlands). Poly(ethylene oxide) (PEO) standard (M_n: 19 kDa, PDI: 1.04) for Viscotek calibration was a product of Malvern Instruments Ltd (Worcestershire, UK). Primary FR polyclonal antibody (FL-257) and the secondary anti-rabbit IgG-Phycoerythrin (IgG-PE0) were obtained from Santa Cruz Biotechnology (Heidelberg, Germany). Wheat germ

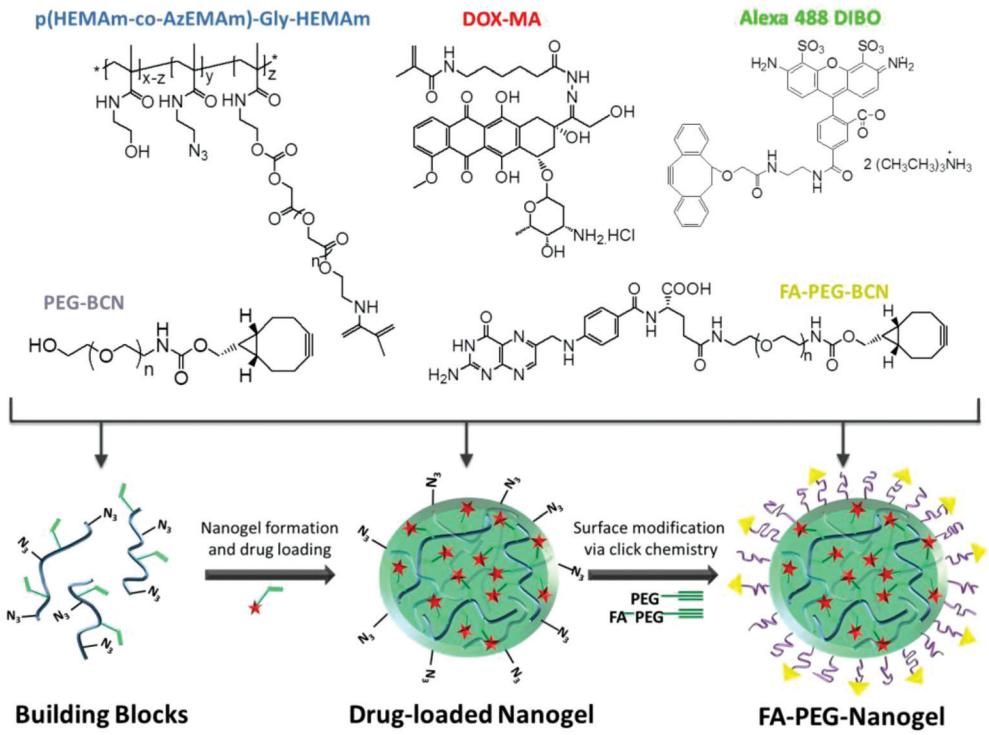

Fig. 1 Chemical structures of the building blocks and nanogels used in present study.

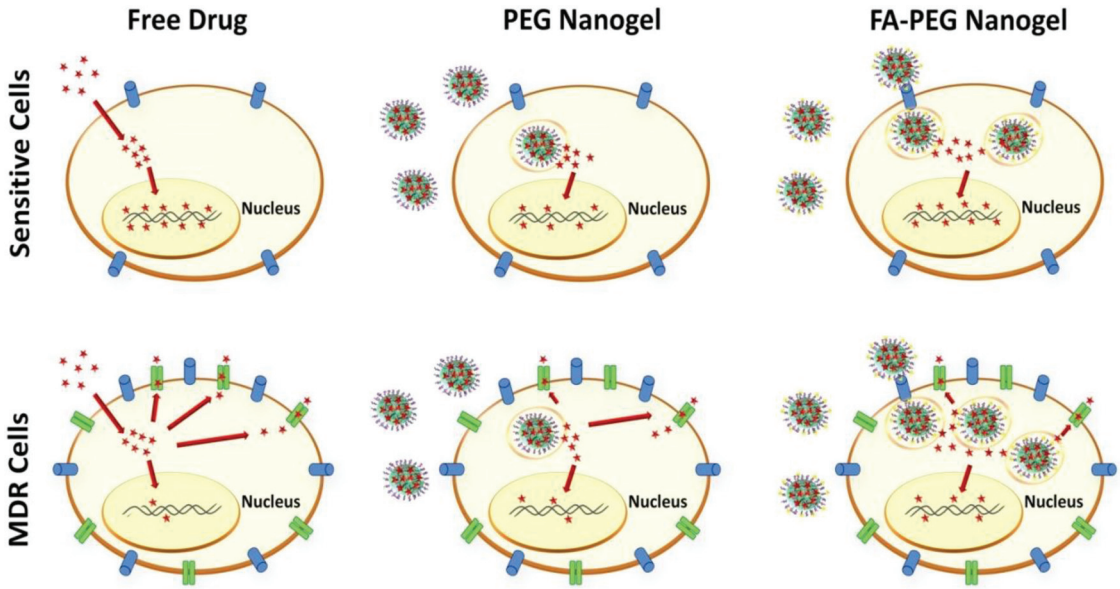

Fig. 2 Schematic depiction of free drug (DOX; ★) *versus* DOX-loaded PEGylated and DOX-loaded FA-PEG (🔻) modified actively targeted nanogels in drug sensitive and MDR cells is shown. The free drug enters the cells *via* passive diffusion through the cellular membrane. In MDR cells, drugs are recognized and externalized by efflux pumps (▮). PEGylated nanogels are taken up by cells and end up in late endosomes/lysosomes. FA-PEG modified nanogels can bind to the upregulated folate receptor (▮) in MDR cells more than in DOX-sensitive cells. The internalized nanogels enable pH-sensitive DOX release in late endosomes/lysosomes at the perinuclear region. Hence released DOX can pass through the nuclear envelope and intercalate into DNA where it exerts its pharmacological action.

agglutinin (WGA), RPMI-1640 medium, Dulbecco's Modified Eagle's medium (DMEM), sodium pyruvate solution (100 mM), fetal bovine serum (FBS), Hoechst 33342 solution (20 mM), LysoTracker® Depp Red (1 mM) and Alexa Fluor® 488 DIBO Alkyne were purchased from ThermoFisher (Bleiswijk, the Netherlands). All other chemicals and reagents were obtained from Sigma-Aldrich (Zwijndrecht, the Netherlands).

2.2 NMR, UPLC and GPC analysis

^{1}H-NMR spectra of the different synthesized compounds dissolved in DMSO-d_6 or deuterium oxide were recorded using an Agilent 400-NMR spectrometer (Santa Clara, CA, USA). The central line of DMSO at 2.49 ppm or deuterium oxide at 4.75 ppm was used as reference line.

Determination of HEMAm, *N*-(2-azidoethyl)methacrylamide (AzEMAm), DOX and DOX-MA was performed on a Waters ACQUITY UPLC system (Waters Associates Inc., Milford, MA) using an Acquity BEH C18 column 1.7 μm (2.1 × 50 mm). The chromatograms were analyzed by Empower Software.

For HEMAm and AzEMAm, 10 mM $HClO_4$/acetonitrile (95/5, v/v) was used as eluent A and 10 mM $HClO_4$/acetonitrile (5/95, v/v) was used as eluent B. The injection volume was 5 μL and the detection wavelength was 210 nm. After an isocratic flow of eluent A for 1 min, a gradient was run from 100% to 50% eluent A in 2 min with a flow rate of 0.5 mL min^{-1}. The retention times of HEMAm and AzEMAm were 0.78 and 2.11 min, respectively. Calibration curves were linear between 0.01 and 10 μg mL^{-1} for both HEMAm and AzEMAm.

For the analysis of DOX and DOX-MA, potassium phosphate buffer (20 mM, pH 3)/acetonitrile (75/25, v/v) was used as the eluent. The injection volume was 5 μL and fluorescence detection was performed using 480 and 560 nm as excitation and emission wavelength, respectively. The retention time of DOX was 1.30 min and that of DOX-MA was 2.39 min. Calibration curves were linear between 0.1 and 10 μg mL^{-1} for both DOX and DOX-MA in ammonium acetate buffer (100 mM, pH 5) and HEPES buffer (300 mM, pH 7.4), respectively.

Molecular weight and molecular weight distribution of the synthesized polymers were determined using Viscotek TDAmax (equipped with refractive index, light scattering and viscosity detectors, Malvern Instruments Ltd, UK) with two PL aquagel-OH 30 columns (Agilent, USA). A 0.3 M sodium acetate buffer (pH 6.5) was used as the eluent with a flow rate of 0.7 mL min^{-1}. Samples were dissolved in the mobile phase and injected onto the column (injection volume 100 μL). Results were analyzed by OmniSEC software (Malvern Instruments Ltd, UK) with poly(ethylene oxide) (M_n: 19 kDa, PDI: 1.04) as the calibration standard.

Determination of the concentration of PEG_{5000}-BCN was performed by Viscotek TDAmax with a PL aquagel-OH 30 column, using HEPES buffer (100 mM, pH 7.4) as the eluent. The flow rate was 0.7 mL min^{-1} and the light scattering signal was recorded. The calibration curve was linear between 1 and 10 mg mL^{-1}.

2.3 Synthesis and characterization of the building blocks of the nanogels

2.3.1 Synthesis and characterization of p(HEMAm-*co*-AzEMAm)-Gly-HEMAm. Synthesis of the monomer *N*-(2-azidoethyl)methacrylamide (AzEMAm) was carried out as

described before[28,29] with some modifications. The detailed synthesis is described in the ESI.† The final product was characterized by ^{1}H-NMR using deuterium oxide as the solvent.

For the synthesis of p(HEMAm-*co*-AzEMAm), 4,4-azobis(4-cyanopentanoic acid) (ABCPA, 45.3 mg, 0.16 mmol), HEMAm (250 mg, 1.94 mmol) and AzEMAm (75 mg, 0.49 mmol) were dissolved in 10 mL deionized water, followed by 30 min flushing with N_2 gas. The polymerization was performed at 70 °C for 24 h. Next, 5 μL reaction mixture was taken and analyzed by UPLC for determination of the conversion of the monomers. The polymer was obtained after dialysis against deionized water and lyophilization. The polymer was characterized by FT-IR analysis, and the mole percentage AzEMAm in the polymer and the conversions of monomers were determined and calculated (see the ESI†). The molecular weight and molecular weight distribution of p(HEMAm-*co*-AzEMAm) were determined by Viscotek as in section 2.2.

p(HEMAm-*co*-AzEMAm)-Gly-HEMAm with a degree of substitution (DS, the number of methacryloyl groups per 100 HEMAm units) of approximately 10 was prepared as previously described.[24] Briefly, CDI activated HEMAm-Gly (HEMAm-Gly-CI) was obtained by reaction of the hydroxyl group of HEMAm-Gly (degree of polymerization 1.83) with CDI.[25] Subsequently, HEMAm-Gly-CI was coupled to p(HEMAm-*co*-AzEMAm) catalyzed by DMAP.[24]

2.3.2 Synthesis and characterization of folic acid-polyethylene glycol-bicyclo[6.1.0]nonyne (FA-PEG-BCN). FA-PEG-BCN was synthesized in three steps (Scheme S1†). First folic acid was activated by NHS and reacted with the free amine group of NH_2-PEG-NH-Boc.[30–32] Then the protective Boc group was removed and finally BCN was reacted with the amine group of PEGs. The detailed synthesis is described in the ESI.†

The synthesized FA-PEG conjugates were characterized by ^{1}H-NMR using DMSO-d_6 as solvent.

GPC analysis of the FA-PEG conjugates was performed using a Waters System (Waters Associates Inc., Milford, MA) with refractive index (RI) and UV detection using a PLgel 5 μm MIXED-D column (Agilent, USA) and DMF with 10 mM LiCl as eluent. The injection volume was 100 μL. The flow rate was 1 mL min^{-1} and the temperature was 60 °C. UV detection of FA was done at 350 nm.

To calculate the conjugation efficiency, FA-PEG conjugates were dissolved in DMSO at a concentration of 1 mg mL^{-1} and the absorbance at 350 nm was recorded using an ultraviolet-visible (UV-vis) spectrophotometry (BMG Labtech, Germany). The amount of conjugated FA was calculated using a calibration curve of FA in DMSO which was linear between 10 and 100 μg mL^{-1}. FA mol% was calculated as eqn (1)

$$\text{FA mol\%} = \frac{\text{amount of conjugated FA/molecular weight of FA}}{\text{amount of FA-PEG/molecular weight of FA-PEG}} \times 100\% \quad (1)$$

2.4 Preparation and characterization of nanogels

2.4.1 Preparation of DOX-loaded nanogels (DOX-NG). Inverse mini-emulsion photopolymerization was used to prepare DOX loaded nanogels (DOX-NG) essentially as described previously.[24,33] In short, p(HEMAm-*co*-AzEMAm)-Gly-HEMAm (37.5 mg, section 2.3.1) was dissolved in 212.5 μL DMSO and mixed with 200 μL of DOX-MA (20 mg mL^{-1} in DMSO). Subsequently, 150 μL of Irgacure 2959 (10 mg mL^{-1} in 20 mM HEPES, pH 7.4) was added. This solution (to form the internal phase) was added to 5 mL external phase (mineral oil containing 10% v/v ABIL EM 90). An emulsion was formed after ultrasonication (Bandelin Sonopuls, pulse on/off 0.5 s, and amplitude 10%) for 15 min which was subsequently irradiated with UV light (940 mW cm^{-2}, 300–650 nm, Bluepoint UVC source, Honle UV technology, German) for 15 min. Subsequently, 40 mL hexane was added to the emulsion and a pellet was collected after centrifugation (3000*g*, 3 min). The obtained pellet was washed four times with acetone/hexane (40 mL, 1 : 1, v/v) and redispersed in 10 mL distilled water and centrifuged at 250 000*g* (Optima L-90 K Ultracentrifuge, Beckman Coulter, Inc.) for 1 h to remove unreacted DOX-MA. Finally, the obtained pellet was redispersed in 2 mL distilled water and lyophilized.

2.4.2 Preparation of PEGylated nanogels with or without FA (PEG-DOX-NG and FA-DOX-NG). PEGylation of the nanogels was done using a copper-free click chemistry reaction between the BCN group of PEG or FA-PEG conjugate and azide groups of the nanogels.[34–36] Freeze dried particles (prepared as described in section 2.4.1; 10 mg) were dispersed in 2 mL of HEPES buffer (300 mM, pH 7.4) and 1 mL PEG-BCN or FA-PEG-BCN solution (10 mg mL^{-1} in HEPES buffer) was added. The mixture was stirred for 4 h at 4 °C in the dark. Next, unreacted PEG-BCN or FA-PEG-BCN were removed by washing the nanogel particles 3 times after ultracentrifugation (250 000*g* for 1 h). PEG-DOX-NG or FA-DOX-NG was obtained after freeze drying.

2.4.3 Characterization of the different nanogels. To determine the conversion of methacrylamide units after photopolymerization, freeze-dried nanogels were dispersed in 0.02 M NaOH at a concentration of 1 mg mL^{-1} and incubated at 37 °C. Next, 0.2 mL sample was withdrawn and mixed with 0.5 ml of sodium acetate buffer (1 M, pH 5.0). The amount of unreacted HEMAm was determined by UPLC (see section 2.2).[37]

The size and size distribution of re-suspended nanogels (0.5 mg mL^{-1} in 20 mM HEPES pH 7.4) were measured by dynamic light scattering (DLS, Malvern ALV/CGS-3 Goniometer, Malvern, UK) at 25 °C. The zeta potential of the nanogels in 20 mM HEPES (pH 7.4) was measured using a Malvern Zetasizer Nano-Z (Malvern, UK) at 25 °C.

To determine the amount of DOX loaded in the nanogels, a sample of freeze dried particles (around 5 mg, accurately weighed) was dispersed in pH 5 ammonium acetate buffer (100 mM) at a concentration of 0.5 mg mL^{-1} and incubated at 37 °C for 24 h. This time is sufficient to hydrolyze the hyrazone

bond that connects DOX to the nanogel network.[38,39] The concentration of DOX in the supernatant after centrifugation at 20 000*g* for 60 min was measured by UPLC (see section 2.2). Loading capacity (LC) and encapsulation efficiency (EE) were calculated using eqn (2) and (3).

$$\mathrm{LC} = \frac{\text{weight of DOX in the supernatant}}{\text{weight of DOX loaded nanogels}} \times 100\% \quad (2)$$

$$\mathrm{EE} = \frac{\text{weight of loaded DOX}}{\text{weight of feed DOX}} \times 100\% \quad (3)$$

After modification of DOX-NG with PEG or FA-PEG, the amount of unreacted PEG/FA-PEG-BCN was determined by Viscotek and UV analysis, respectively (see section 2.2). The modification efficiency (ME) was calculated using eqn (4).

$$\mathrm{ME} = \frac{\text{amount of added (PEG or FA-PEG-BCN)} - \text{amount of unreacted (PEG or FA-PEG-BCN)}}{\text{amount of added (PEG or FA-PEG-BCN)}} \times 100\% \quad (4)$$

2.4.4 Stability of the different nanogels in cell culture medium. Freeze dried DOX-NG, PEG-DOX-NG and FA-DOX-NG were dispersed in RPMI-1640 medium with or without 10% (v/v) FBS at the concentration of 5 mg mL^{-1} and incubated at 37 °C. After 0 h and 4 h incubation, 0.1 mL suspension was taken and mixed with 0.9 mL of sodium acetate buffer (1 M, pH 5.0). Size distribution was determined by DLS at 25 °C.

2.4.5 Preparation of Alexa 488 labeled nanogels. Labeling of FA-DOX-NG was performed using copper-free click chemistry between the DIBO group of the dye and azide groups on the nanogels.[40] In short, freeze dried FA-DOX-NG (10 mg) were dispersed in 1 mL of HEPES buffer (20 mM, pH 7.4). Next, 10 μL of Alexa 488 DIBO (1 mg mL^{-1} in DMSO) was added. The mixture was stirred at 4 °C for 1 h, followed by the purification PD 10 column chromatography. The labelled FA-DOX-NG was obtained after freeze drying.

2.4.6 *In vitro* DOX release. DOX-MA (20 μg mL^{-1}) and nanogels (DOX-NG, PEG-DOX-NG and FA-DOX-NG, 1 mg mL^{-1}) were dissolved/dispersed in an ammonium acetate buffer (100 mM, pH 5.0) and HEPES buffer (300 mM, pH 7.4), and subsequently incubated at 37 °C. At different time points, 200 μL samples were taken and centrifuged (20 000*g*, 60 min) at 4 °C. The supernatant was analyzed by UPLC for DOX concentration (see section 2.2).

2.5 Cell culture

Murine melanoma cells B16F10 were maintained in Dulbecco's modified Eagle's medium (DMEM) supplemented with sodium pyruvate (final concentration 1 mM) and fetal bovine serum (FBS, final concentration 10% v/v). Human lung carcinoma A549 cells were cultured in DMEM supplemented with FBS (final concentration 10% v/v). DOX-sensitive 4T1 cells were cultured in RPMI-1640 medium (GibcoBRL, USA) with 10% fetal bovine serum in a cell incubator at 37 °C. The DOX resistant 4T1 cell line was developed from the sensitive parental 4T1 cells with low dose of free DOX administration which was further followed by stepwise increase.[8] For this process, starting dose (IC90 concentration; enabling the survival of 10% of the population) was detected according to the XTT cytotoxicity test. The cells were cultured in a humidified atmosphere containing 5% CO_2 at 37 °C.

2.6 Folate receptor immunostaining

B16F10, A549, and sensitive and resistant 4T1 cells were seeded in a 24-well plate for 24 h in DMEM medium (for B16F10 and A549 cells) and RPMI medium 1640 (for 4T1 cells) with 10% FBS. The cells were subsequently washed with PBS, fixed with 4% paraformaldehyde and incubated with 5% BSA for 1 h for blocking. After washing with PBS, the cells were incubated with primary FR polyclonal antibody (1 : 100 dilution in PBS) for 2 h at room temperature. Subsequently, the cells were incubated with the secondary anti-rabbit IgG-Phycoerythrin (IgG-PE0) (1 : 500 dilution in PBS), DAPI and WGA for 30 min. Cells were washed and mounted with 50% glycerol, and folate receptor expression was visualized under a fluorescence microscope (Zeiss, Germany). Digital images were acquired using three channels: a DAPI channel ($\lambda_{ex.}$ 365 nm, $\lambda_{em.}$ 455 nm) for nuclei, an IgG-PE0 channel ($\lambda_{ex.}$ 488 nm, $\lambda_{em.}$ 560 nm) for the folate receptor and a WGA channel ($\lambda_{ex.}$ 495 nm, $\lambda_{em.}$ 518 nm) for cell membranes. The images were analyzed by the software ImageJ and relative area fraction of IgG-PE0 channel was calculated.

2.7 Drug efflux pump (P-glycoprotein; P-gp) expression levels in DOX-sensitive and -resistant 4T1 cells

MDR1 (the gene encoding P-gp protein) mRNA expression level, in DOX-sensitive and -resistant 4T1 cells, was measured by reverse transcription-polymerase chain reaction (RT-PCR). Total RNA was extracted from cells using the GeneMATRIX Universal RNA purification kit (Roboklon, Germany). The expression levels of MDR1 mRNA were normalized to beta-actin. SsoAdvanced Universal SYBR Green Supermix kit (Bio-Rad, USA) was used for RT-PCR. The sequences of the primers for MDR1 and beta-actin were as follows: MDR1- (forward): 5′-CCCATCATTGCAATAGCAGG-3′, (reverse): 5′-GTTCAAACTTCT GCTCCTGA-3′; beta-actin- (forward): 5′-CTCTAGACTTCGAG CAGGAGATGG-3′, (reverse): 5′-ATGCCACAGGATTCCCATACCC AAGA-3′. The RT-PCR conditions were also as follows: polymerase activation and DNA denaturation at 95 °C for 30 s, followed by amplification for 40 cycles, each cycle includes denaturation at 95 °C for 10 s, annealing and extension at 60 °C for 30 s. As a final stage, melt curve analysis took place in an increasing way of 0.5 °C each 5 s per step starting up from

65 °C to 95 °C. The expression of the target gene was calculated using ΔΔCT method.[41]

Immunostaining was performed for the DOX-sensitive and -resistant 4T1 cells to detect the P-gp protein level. 1×10^5 cells per well were seeded in a 24-well plate in RPMI 1640 with 10% FBS. After overnight incubation, cells were washed with PBS solution. The cells were, then, fixed with 4% paraformaldehyde and incubated with 5% BSA for 1 h for blocking. After washing with PBS, the cells were incubated with primary P-gp monoclonal antibody (1 : 100 dilution in PBS) for 2 h at room temperature. After washing with PBS two times, the cells were incubated with the secondary anti-rabbit IgG (Alexa Fluor 488 carboxylic acid) (1 : 500 dilution in PBS) and DAPI for 30 min. Cells were washed and mounted with 50% glycerol, and P-gp expression was visualized under a fluorescence microscope (Zeiss, Germany). Digital images were acquired using two channels: a DAPI channel ($\lambda_{ex.}$ 365 nm, $\lambda_{em.}$ 455 nm) for nuclei, and GFP channel ($\lambda_{ex.}$ 470 nm, $\lambda_{em.}$ 525 nm) for the P-gp. The images were analyzed by the software ImageJ and the relative area fraction of P-gp was calculated.

2.8 Cell studies on B16F10 and A549 cells

2.8.1 Cellular uptake of DOX, DOX-MA and DOX-loaded nanogels by B16F10 and A549 cells. Uptake of free DOX, DOX-MA and the different nanogel formulations by B16F10 and A549 cells was monitored by Yokogawa high content screening system. Briefly, B16F10 and A549 cells were seeded into a 96-well plate at density of 2×10^4 and 5×10^4 cells per well respectively, and incubated for 24 h at 37 °C. Free DOX, DOX-MA or nanogels at a concentration of 1000 nM equivalent DOX for B16F10 and 3000 nM for A549 were added and incubated for 24 h at 37 °C. Subsequently, the cells were washed with PBS for three times and Hoechst 33342 (1 : 1000 dilution in PBS) was added to the wells 30 min before imaging (final concentration was 10 nM) to stain the nuclei of the cells. The plate was subsequently transferred into the microscope. Digital images were collected using two channels: a channel ($\lambda_{ex.}$ 405 nm, $\lambda_{em.}$ 445 nm) for nuclei and another channel ($\lambda_{ex.}$ 488 nm, $\lambda_{em.}$ 600 nm) for DOX. The fluorescence intensity of DOX in the cells was quantified by the ImageJ software.

2.8.2 Uptake kinetics of DOX and FA-DOX-NG by B16F10 cells. The real-time kinetics of uptake of both free DOX and FA-DOX-NG by cells was studied using a high content screening system with a confocal scanner unit, a live cell stage incubator and a build-in liquid handler (Yokogawa CV7000S). In detail B16F10 cells were seeded into a 96-well plate at a density of 2×10^4 cells per well. After 24 h incubation, Hoechst 33342 (1 : 1000 dilution in PBS) was added to the wells (final concentration was 10 nM) and incubated with the cells for 30 min at 37 °C to stain the nuclei of the cells. Then, the medium was removed, and free DOX and FA-DOX-NG (25 000 nM equivalent DOX) were added. The plate was transferred and incubated in Yokogawa (37 °C, 5% CO_2). Digital images were acquired every 10 min for 1 h using two channels: a channel ($\lambda_{ex.}$ 405 nm, $\lambda_{em.}$ 445 nm) for nuclei and another channel ($\lambda_{ex.}$ 488 nm, $\lambda_{em.}$ 600 nm) for DOX. The fluorescence intensity of DOX in nucleus and cytoplasm was quantified by the ImageJ software.

2.8.3 Subcellular distribution of FA-DOX-NG on B16F10 cells. To investigate the subcellular distribution of DOX and nanogels, B16F10 cells were seeded into a 96-well plate at a density of 2×10^4 cells per well and incubated at 37 °C for 24 h. Alexa 488 labeled FA-DOX-NG (12 500 nM equivalent DOX) was added and incubated at 37 °C for 6 h. Subsequently, Hoechst 33342 (1 : 1000 dilution in PBS) and Lysotracker Deep Red (1 : 1000 dilution in PBS) were added to each well 30 min before imaging, with final concentrations of 10 and 50 nM, respectively. The cells were washed with PBS three times and the plate was transferred into Yokogawa high content screening system. Digital monochromatic images were acquired using a Hoechst channel ($\lambda_{ex.}$ 405 nm, $\lambda_{em.}$ 445 nm) for nuclei, a DOX channel ($\lambda_{ex.}$ 488 nm, $\lambda_{em.}$ 600 nm) for DOX, a Alexa 488 channel ($\lambda_{ex.}$ 488 nm, $\lambda_{em.}$ 525 nm) for nanogels and a Lysotracker channel ($\lambda_{ex.}$ 640 nm, $\lambda_{em.}$ 676 nm) for late endosomes/lysosomes. Colocalization was further assessed by calculating Pearson correleation coefficient (PCC) of different channels: nuclei and late endosomes/lysosomes, nanogels and late endosomes/lysosomes, nanogels and nuclei, DOX and late endosomes/lysosomes, DOX and nanogels, and DOX and nuclei. The calculation was done by the ImageJ software[42] and PCC was defined as follows: −1, perfect negative correlation; 0, no correlation; 1, perfect positive correlation.[43]

2.8.4 Cytotoxicity in B16F10 and A549 cells. B16F10 (5×10^3 cells per well) and A549 (1×10^4 cells per well) were seeded into 96-well plates and cultured overnight at 37 °C in a humidified atmosphere containing 5% CO_2. Medium was removed and 200 μL of free DOX, DOX-MA or DOX nanogels in medium was added to the wells at a concentration of DOX equivalents between 2 and 250 000 nM. After 72 h of incubation at 37 °C, 40 μL of MTS reagent was added to the wells and the MTS assay was performed according to manufacturer's protocol. The absorbance at 492 nm was recorded using a reference wavelength of 690 nm.

2.8.5 Competitive inhibition. B16F10 (5×10^3 cells per well) and A549 (1×10^4 cells per well) were seeded into 96-well plates 24 h before feeding the formulations. Then, the culture medium was replaced by free DOX, PEG-DOX-NG and FA-DOX-NG in medium with or without 1 mM folic acid (the molar ratio of free and conjugated FA > 100). The final DOX concentration was 100 nM for B16F10 and 1900 nM for A549. Cells were incubated in a humidified atmosphere containing 5% CO_2 at 37 °C for 72 h after which the cell viability was recorded by the MTS assay.

2.9 Cellular uptake and cytotoxicity in DOX-sensitive and resistant 4T1 cells

2.9.1 Uptake of DOX, DOX-MA and DOX-loaded nanogel formulations by DOX-sensitive and -resistant. 4T1 cells DOX-sensitive or -resistant 4T1 cells (1×10^5 cells per well) were seeded in a 24-well plate in RPMI 1640 with 10% FBS. After 24 h, the cells were incubated with free DOX, DOX-MA and nanogel formulations (300 000 nM equivalent DOX) for 24 h at

37 °C. Next, the cells were washed with PBS and fixed with 4% formaldehyde solution in PBS. Nuclear and cytoplasm staining was performed by incubation for 15 min with Hoechst 33342 (1 : 200 dilution) and WGA (1 : 500 dilution), respectively. Fluorescence microscopy were taken on the confocal microscope ($\lambda_{ex.}$ 405 nm and $\lambda_{em.}$ 445 nm for Hoechst; $\lambda_{ex.}$ 488 nm and $\lambda_{em.}$ 560 nm for DOX; $\lambda_{ex.}$ 495 nm and $\lambda_{em.}$ 519 nm for cell membranes). Relative accumulation of DOX in cells was analyzed by ImageJ software.

2.9.2 Cytotoxicity in DOX-sensitive and -resistant 4T1 cells. The XTT assay was used to determine the cytotoxicity of free DOX, DOX-MA and nanogel formulations in sensitive and resistant 4T1 cells. Cells were seeded into 96-well plates at 1×10^4 cells per well with the final volume of 200 μL. After 24 h, the medium was refreshed with 200 μL folic acid-free medium and 100 μL of free DOX, DOX-MA or nanogel suspensions in PBS was added to a final DOX equivalent concentration ranging from 10 to 300 000 nM. After 72 h incubation at 37 °C, 50 μL of a freshly prepared XTT solution (25 μM *N*-methyl dibenzopyrazine methylsulfate (PMS) and 1 mg mL^{-1} 2,3-bis(2-methoxy-4-nitro-5-sulfophenyl)-2*H*-tetra-zolium-5-carboxanilide (XTT) in plain RPMI 1640 medium) was added to each well. The cells were incubated for 2 h at 37 °C in a CO_2 incubator. The absorbance was read at 475 nm with a reference wavelength of 660 nm.

Resistance index (RI) of all formulations was calculated according to eqn (5):

$$\mathrm{RI} = \frac{\mathrm{IC_{50}\ on\ resistant\ cells}}{\mathrm{IC_{50}\ on\ sensitive\ cells}}. \quad (5)$$

2.10 Statistics

All results are presented as mean ± standard deviation. The two-tailed Student's test was used to determine significance between groups. Significant differences were considered when $p < 0.05$.

3 Results and discussion

3.1 Synthesis and characterization of the building blocks of the nanogels

3.1.1 Synthesis of p(HEMAm-*co*-AzEMAm)-Gly-HEMAm. AzEMAm (Scheme S2A†), an azide monomer, was synthesized as shown in Scheme S2A,† using the protocol for the synthesis of *N*-(3-azidopropyl) methacrylamide[28] with some slight modifications. In the first step, 2-bromoethylamine was converted into the azido-derivative by reaction with sodium azide (38.6% yield). Next, the obtained 2-azidoethanamine was reacted with methacryloyl chloride. After purification by flash chromatography, the desired monomer AzEMAm was obtained in 44.1% yield.

^{1}H-NMR AzEMAm (Fig. S1,† DMSO-d_6, 400 MHz): δ 5.69 (s, 1H, H_a), 5.45 (s, 1H, $H_{a'}$), 3.54–3.36 (m, 4H, H_c, H_d), 1.91 (s, 3H, H_b).

P(HEMAm-*co*-AzEMAm) was synthesized by free radical polymerization using HEMAm and AzEMAm as monomers and ABCPA as initiator (Scheme S2B†). The characteristics of the obtained polymer are summarized in Table S1.† HPLC analysis showed high conversions of both HEMAm and AzEMAm (>95%) and the polymer was obtained in a high yield (>90%). A resonance peak at 3.46 ppm (Fig. S2†) is found in the NMR spectrum of p(HEMAm-*co*-AzEMAm), which is assigned to the methyl protons at the β position to the azide group. Using eqn (1) it is calculated that the obtained polymer contains 21% of AzEMAm which corresponds well with the feed ratio of AzEMAm and HEMAm (20/80) and can be expected for a polymer obtained in a high yield. The obtained copolymer had a number average molecular weight (M_n) of 15 kDa with a PDI of 3, which is typical for polymers synthesized by free radical polymerization. The FT-IR spectrum of p(HEMAm-*co*-AzEMAm) showed a peak at 2100 cm^{-1} characteristic for the azide vibration (Fig. S3†). In the next step, the obtained p(HEMAm-*co*-AzEMAm) was further modified with biodegradable and polymerizable side units HEMAm-Gly and used as building block for the nanogel particles the obtained polymer was modified with polymerizable methacrylamide groups (HEMAm-Gly) after activation of the hydroxyl group of HEMAm-Gly with 1,1′-carbonyldiimidazole using a previously established method (Scheme S2C†) to obtain p(HEMAm-*co*-AzEMAm)-Gly-HEMAm (93.5% yield).[24] NMR analysis showed that the degree of substitution was around 10 (Scheme S2C,† p(HEMAm-*co*-AzEMAm)-Gly-HEMAm). The azide groups of the polymer provide the opportunity for modification of the nanogels with functional moieties with alkynes using so-called click chemistry.[36]

3.1.2 Synthesis and characterization of folic acid-PEG conjugate. To obtain actively targeted nanogels, a folic acid-PEG functionalized with an alkyne group was synthesized as follows. First, a heterobifunctional PEG (NH_2-PEG-NH-Boc) was reacted with FA after activation of its γ-carboxylic acid group (which has a higher reactivity than the α-carboxylic acid group[44,45]) with NHS. Next, the Boc group was removed under mild acidic conditions and the BCN group was introduced *via* the reaction of BCN-NHS and the formed amine of PEG.

^{1}H-NMR and GPC data revealed that FA was indeed successfully conjugated to PEG. In the ^{1}H-NMR spectra of the obtained products (Fig. S4†), weak signals at 6.5–8.5 ppm corresponding to the aromatic protons of FA were detected after the first reaction and were also present in both the other intermediate and final product. After deprotection, the peaks at 1.3 ppm assigned to the Boc group disappeared completely. Finally, new peaks at 1.2–2.3 ppm ascribed to BCN (protons of the eight-membered ring) introduced after the reaction of FA-PEG-NH_2 with BCN-NHS were detected. To prove that FA was indeed covalently coupled to PEG, GPC analysis was performed using UV (350 nm) and RI detection (Fig. S5†). The physical mixture had a peak at 8 min (RI detection) for PEG and at 12 min (UV detection) for FA. Importantly, after reaction of FA and PEG, the product displayed peaks at 8 min both with RI and UV detection, demonstrating that FA was indeed co-

valently coupled to PEG. The chromatogram (Fig. S5A†) shows a small shoulder (retention time around 7.5 min for both RI and UV detection). Likely, NH_2-PEG-NH-Boc has reacted with both carboxylic acids of FA, which doubled the molecular weight of PEG.

UV-vis spectroscopic analysis showed that the FA mol% of FA-PEG-BCN was around 60%.

3.2 Preparation and characterization of DOX-loaded nanogels

Inverse mini-emulsion photopolymerization[24,33] was used to prepare DOX-loaded nanogels (DOX-NG). The irradiation conditions were optimized for high conversion of the methacrylamide groups, and simultaneously to minimize possible UV-catalyzed degradation of DOX-MA.[46] Under the optimized reaction condition (940 mW cm^{-2}, 300–650 nm, 15 min), relatively high conversion of methacrylamides (71.7 ± 2.1%) and high encapsulation efficiency of DOX (72.1 ± 2.8%) was obtained. The size of DOX-NGs was around 170 nm with a PDI 0.21 as determined by DLS; the zeta potential of the nanogels in HEPES buffer (pH 7.4) was slightly negative (Table 1).

PEGylation with and without FA decoration of DOX-NG using copper-free click chemistry was performed at pH 7.4 to avoid drug release caused by the cleavage of the hydrazone bond of DOX-MA which is labile under acid conditions.[38] Since glycolate esters in the crosslinks can be hydrolyzed at this pH,[47,48] a low temperature and short reaction time were used to minimize degradation of the nanogels. The degree of modification with PEG and FA as calculated by determination of unreacted PEG or FA-PEG (eqn (4)) was 67.3% and 80.4% respectively (Table 1), indicating high reaction efficiency and specificity of this reaction as reported in other studies.[49,50] After PEGylation the size of particles slightly increased from 167 to 178 nm likely due to the thickness of PEG coating.[51] The zeta potential of nanogels after PEGylation and FA decoration remained close to neutral. LC of PEG-DOX-NG (3.2%) or FA-DOX-NG (3.0%) was found to be smaller than DOX-NG (5.4%). This is because the total amount of modified nanogels was bigger than unmodified nanogels when the same amount of drug was loaded.

Table 1 Characteristics of drug-loaded nanogels before and after surface functionalization (n = 3)

	LC%	Size (nm)	PDI	Zeta potential (mV)	ME%
DOX-NG	5.4 ± 0.2	167 ± 5	0.21 ± 0.04	−3.2 ± 0.1	—
PEG-DOX-NG	3.2 ± 0.1	178 ± 3	0.17 ± 0.03	−3.0 ± 0.1	67.3 ± 5.6
FA-DOX-NG	3.0 ± 0.1	173 ± 3	0.19 ± 0.04	−4.2 ± 0.1	80.4 ± 4.4

LC: loading capacity, PDI: polydispersity index, ME: modification efficiency.

3.3 Nanogel stability in cell culture medium

Size distributions of the different nanogels before and after incubation in cell culture medium with and without 10% serum were studied. Fig. 4A shows that no big change in size distribution was found for all formulations after incubation in the medium without serum. However, after 4 h incubation in the medium with 10% FBS, DOX-NG showed a new peak with bigger size, indicating some aggregation. On the other hand, PEG-DOX-NG and FA-DOX-NG displayed a similar size distribution. The improved stability can be explained by reduced adsorption of proteins due to the hydrophilic PEG corona.[52]

3.4 Release of DOX from the nanogels

Fig. 3B shows that complete conversion of DOX-MA into DOX was achieved at pH 5 in 8 h, 37 °C, while at pH 7.4 less than

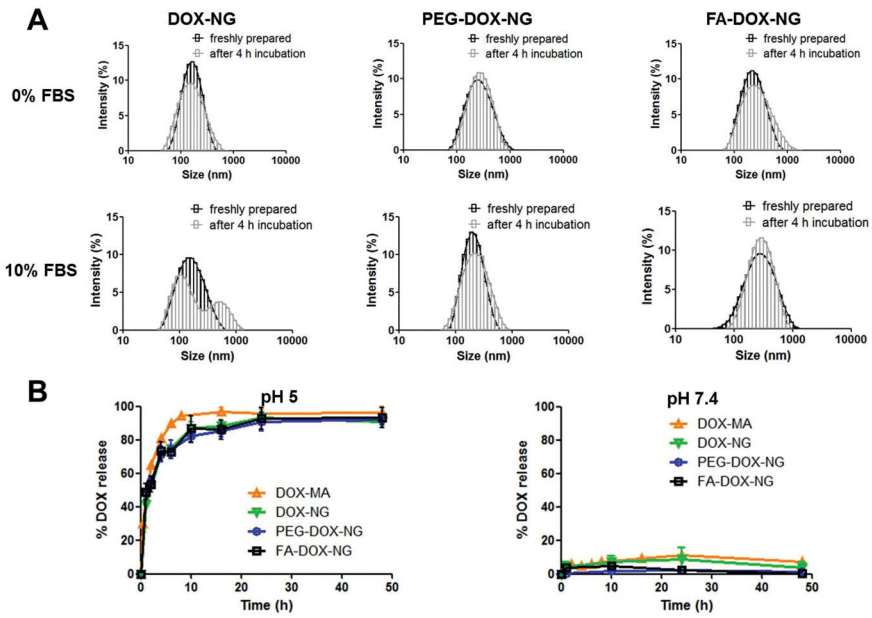

Fig. 3 (A) Size distribution of freshly prepared nanogel formulations and nanogels after 4 h incubation in RPMI-1640 medium with and without 10% FBS at 37 °C. (B) Conversion of DOX-MA into DOX and release of DOX from DOX-MA loaded nanogels at pH 5 and pH 7.4, 37 °C (n = 3).

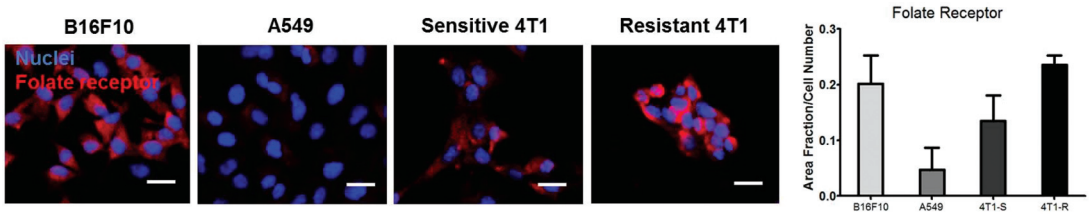

Fig. 4 Immunostaining and quantification of the folate receptor on B16F10, A549, DOX-sensitive and resistant 4T1 cells; nuclei are stained in blue with DAPI and IgG-PE0 is stained in red. Relative area fraction of folate receptor is calculated by the software ImageJ. Bars, 50 μm. The same figures with the green signal from the cell membrane are shown in Fig. S6.†

10% of DOX-MA was converted. This result is in agreement with other studies 27, 38, 39. The DOX-MA loaded nanogels showed a fast drug release at pH 5 (>80% in 10 h) and almost no drug release was found at neutral pH (<10%). Fig. 3B also shows that the release behavior of PEGylated and FA-decorated nanogels was the same as that of the non-PEGylated ones. This can be ascribed to the pH-dependent stability of the hydrazone bond that connects DOX with the nanogel network.

3.5 Folate receptor expression in B16F10, A549, DOX-sensitive and DOX-resistant 4T1 cells

B16F10, A549, DOX-sensitive and -resistant 4T1 cells were incubated with an antibody against the folate receptor and analyzed by confocal microscopy (Fig. 4 and Fig. S6†). B16F10 cells showed strong staining for the folate receptor, while an antibody signal (*i.e.* folate receptor) could hardly be detected for A549 cells. The results of immunostaining showed that B16F10 cells overexpress the folate receptor while A549 cells are folate receptor negative cells, which is in agreement with other studies.[53] The parental (*i.e.* sensitive) 4T1 cells showed strong fluorescence intensity of secondary antibody (Fig. 4), which demonstrates that sensitive 4T1 cells are folate receptor positive cells, in agreement with previous work.[54] DOX resistant 4T1 cells displayed a higher folate receptor expression than the sensitive cells. The observation was further confirmed by the calculation of relative area fraction (right panel, Fig. 4).

3.6 Cell studies with B16F10 and A549 cells

3.6.1 Cellular uptake of DOX-loaded nanogel formulations by B16F10 and A549 cells. The cellular uptake of the different nanogel formulations as well as free DOX and DOX-MA (controls) by B16F10 and A549 cells was investigated using confocal microscopy and using the intrinsic fluorescence of DOX (Fig. 5). To better visualize the DOX signal, higher concentration of DOX was used for A549 (4000 nM) than B16F10 cells (1000 nM).

After 24 h-incubation, B16F10 cells exposed to free DOX showed the highest fluorescence intensity, most of which was in the nucleus. A fluorescence signal was hardly found when the same cells were incubated with DOX-MA. Obviously, the cell membranes are less permeable for DOX-MA than for free DOX. Fig. 5 also shows that B16F10 cells incubated with the different nanogel formulations showed higher fluorescence intensity than those exposed to the same dose of DOX-MA but less than those incubated with free DOX. The internalization of PEG-DOX-NG by B16F10 cells was slightly less (about 70%, Fig. 5B) compared to that of DOX-NG, in agreement with previous studies showing that a PEG corona limits the cellular uptake of nanoparticles.[55,56] However, after decoration of the nanogels with FA (FA-DOX-NG), higher cellular uptake was observed than for the cells incubated with PEG-DOX-NG (almost a factor 2, Fig. 5B). Considering that both PEG-DOX-NG and FA-DOX-NG have a similar size and slightly negative zeta potential (Table 1), the results suggest that the cellular take of nanogels by folate receptor positive cells can be improved by FA decoration.

For A549 cells, the highest and lowest fluorescence intensity was found when the cells were incubated with free DOX and DOX-MA, respectively. However, no big differences in internalization of the different nanogel formulations by A549 cells were observed. This suggests that PEG-DOX-NG and FA-DOX-NG have the same route of uptake in these folate receptor negative cells.

3.6.2 Uptake kinetics of FA-DOX-NG by B16F10 cells. To investigate the uptake kinetics of nanogels as well as free DOX, B16F10 cells were incubated with FA-DOX-NG and real-time images were taken (Fig. 6 and Fig. S7†). Significant difference in uptake pattern of two formulations was observed within one hour incubation with cells. Fast drug accumulation in the nuclei of B16F10 cells (20 min) was observed when the cells were incubated with free DOX (Fig. S7†), which is due to the passive diffusion through the cell and nuclear membrane.[57–59] In contrast, DOX from FA-DOX-NG first accumulated in cytoplasm/endosomes (Fig. 6A, 20 min) and then slowly transferred to nuclei. After 40 min incubation, the fluorescence intensity of DOX in both nucleus and cytoplasm/endosome increased. Quantification of fluorescence intensity of DOX clearly showed that for cells incubated with free DOX, the fluorescence intensity in the nucleus was always much higher than that in cytoplasm at all time points (Fig. S7†) which is in agreement with other studies.[60,61] In contrast, FA-DOX-NG displayed a higher cytoplasm/endosome distribution up to 40 minutes of incubation with cells (Fig. 6B). Besides, the fluorescence intensity of DOX from FA-DOX-NG in both nuclei and cytoplasm/endosomes increased in time (Fig. 6B). However, the rate of increase of fluorescence intensity in the nuclei was higher than in cytoplasm, indicating that the rate of drug release from nanogels was faster than the rate of cellular uptake of

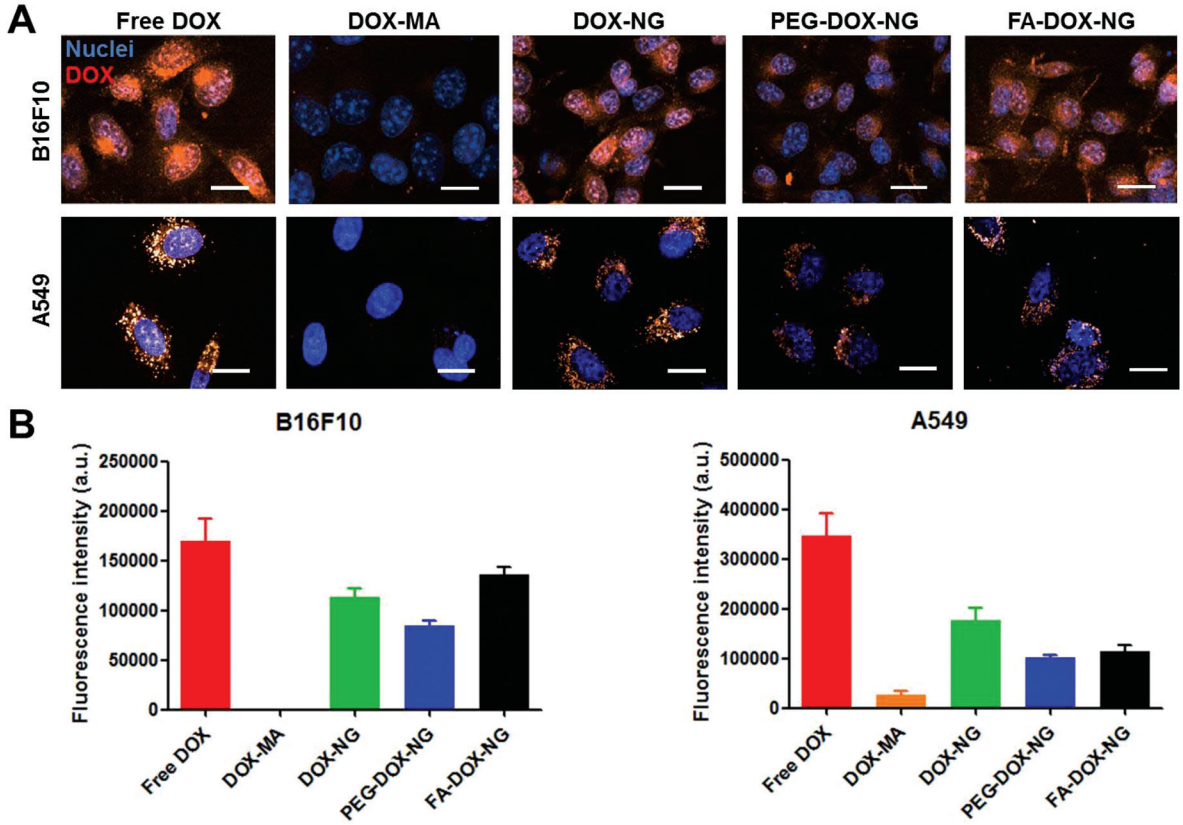

Fig. 5 (A) Confocal microscopy images (DOX is depicted as red and Hoechst (nucleus staining) as blue) and (B) quantification of fluorescence intensity of DOX ($\lambda_{ex.}$ 488 nm, $\lambda_{em.}$ 600 nm) of free DOX, DOX-MA and nanogel formulations by B16F10 and A549 cells at the concentration of 1000 and 4000 nM equivalent DOX, respectively. The incubation time was 24 h. Bars, 20 μm.

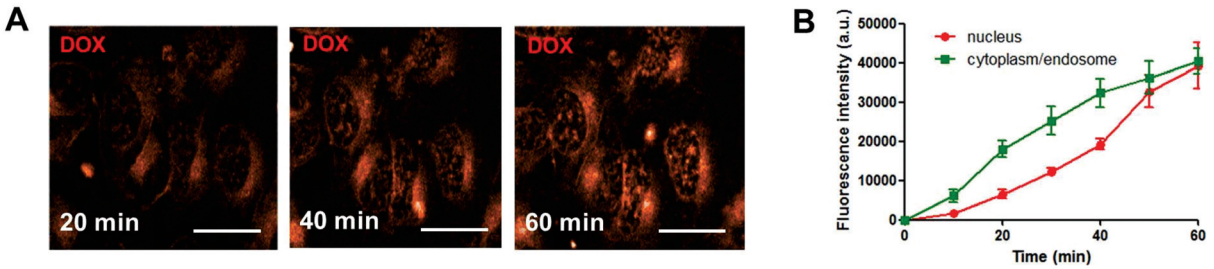

Fig. 6 (A) Confocal microscopy images (DOX is depicted in red) and (B) quantification of fluorescence intensity of DOX ($\lambda_{ex.}$ 488 nm, $\lambda_{em.}$ 600 nm) of uptake kinetics of FA-DOX-NG (25 000 nM equivalent DOX) by B16F10 cells for 1 h at 37 °C. Bars, 20 μm.

nanogels. This result demonstrates that the mechanisms of cellular uptake of free DOX and FA-DOX-NG are different.

3.6.3 Subcellular distribution of FA-DOX-NG in B16F10 cells. Because the DOX signal of FA-DOX-NG observed in the cells by confocal imaging can be from either the encapsulated or the released DOX, FA-DOX-NG covalently labeled *via* a stable triazole bond with Alexa 488 was used to study the fate of DOX and nanogels in the cell separately after cellular internalization. After 6 h incubation, the subcellular distribution of nanogels and DOX was studied by confocal microscope (Fig. 7A, upper panel). Colocalization of the different components was studied by merged images (Fig. 7A, lower panel). By overlapping the images of nanogels and late endosomes/lysosomes, colocalization as indicated by bright yellow, was observed. Exclusion of fluorescent signals was found from the merged image of nuclei and nanogels (Fig. 7A, lower panel). By overlapping the DOX and nanogels signals, partial colocalization (indicated by bright yellow) was observed. Clear drug release was observed from nanogels although there was still a small amount of DOX in the nanogels (Fig. 7A, lower panel). It is also shown that DOX partially colocalized with nuclei (indicated by violet), which can be

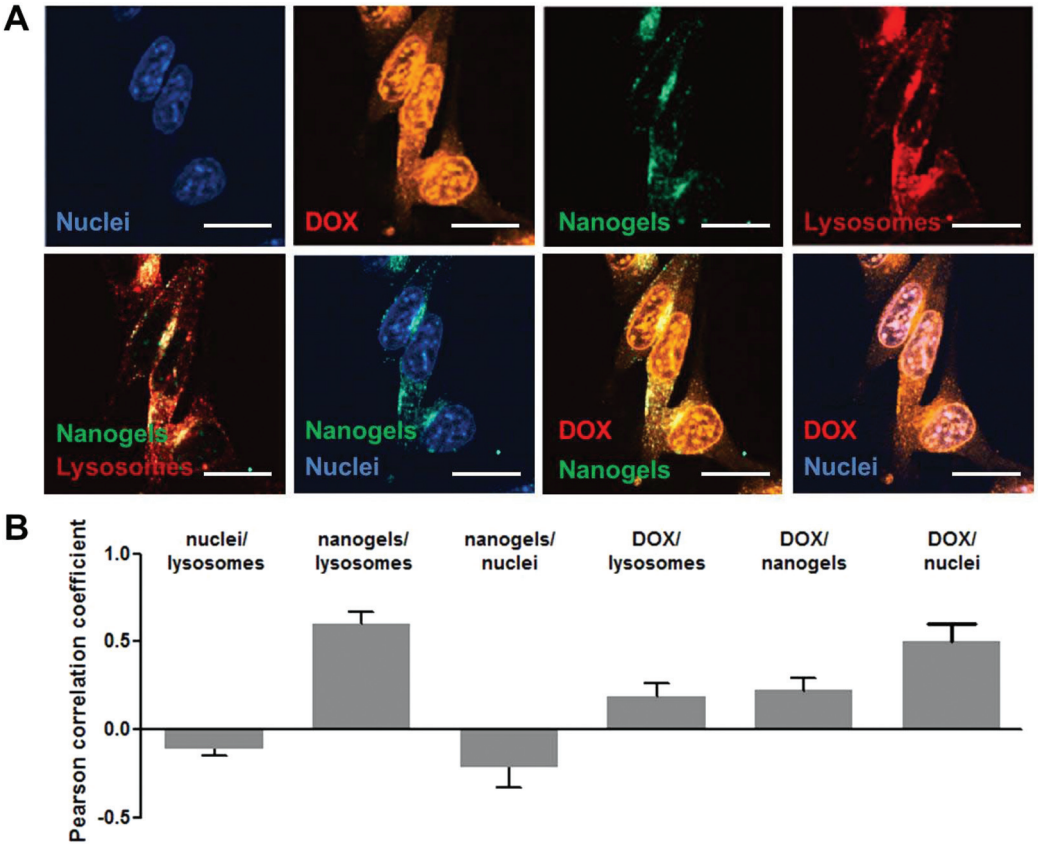

Fig. 7 (A) Confocal images (6 h incubation, Hoechst (nuclear staining) is depicted as blue, Alexa 488 (nanogels) as green, DOX as orange, Lysotracker Deep Red (late endosomes/lysosomes) as red) and (B) colocalization analysis of the different components in B16F10 cells incubated with Alexa 488-labeled FA-DOX-NG (12 500 nM equivalent DOX) at 37 °C. Bars, 20 μm.

observed from the merged image of DOX and nuclei (Fig. 7A, lower panel).

The degree of colocalization was further quantified by calculating Pearson correlation coefficient (PCC, Fig. 7B).[42] The strong colocalization of nanogels and late endosomes/lysosomes (PCC > 0.5) indicates that most of nanogels were located inside late endosomes/lysosomes after 6 h incubation. This result is in agreement with the observation of other studies that the mechanism of cellular uptake of nanomedicines is by endocytosis.[10] A negative PCC, meaning exclusion of the signals, was found for nuclei/lysosomes and nuclei/nanogels, indicating late endosomes/lysosomes and nanogels were not present in the nuclei. The moderate PCC (<0.5) further confirmed partial colocalization of DOX and nanogels. The similar PCC value (<0.5) was also observed for the colocalization analysis of DOX and late endosomes/lysosomes, which is probably due to the DOX still linked to the nanogel network. This also demonstrates that DOX is intracellulary released from the nanogels. Most of DOX signal accumulated in nuclei and a high PCC value (>0.5) was obtained. This observation is in agreement with the result of release study showing that over 70% of DOX was released from nanogels at pH 5 (lysosomal pH) within 6 h (Fig. 3B).

Combining all the results, we can conclude that once incubated with B16F10 cells, FA-DOX-NG can be taken up *via* endocytosis, accumulate in the early endosomes and then end up in the lysosomes. This internalization mechanism is in line with the results of the other studies on nanoparticles and macromolecules.[62] In the late endosomes/lysosomes, DOX is quickly released due to the acidic environment and the released DOX further accumulated into nuclei.[55,63]

3.6.4 Cytotoxicity of DOX-loaded nanogel formulations on B16F10 and A549 cells. The cytotoxicity of free DOX, DOX-MA and the different nanogel formulations was studied using B16F10 cells (folate receptor overexpressing cells) and A549 cells (folate receptor deficient cells) using the MTS assay. The cell viability curves of the different formulations as a function of the DOX concentration are shown in Fig. 8A and the half maximal inhibitory concentrations (IC50) derived from these graphs are reported in Table S2.†

Fig. 8A and Table S2† show that free DOX demonstrated the highest cytotoxicity on both cell lines. The IC50 of DOX-MA (370 ± 30 and 2400 ± 300 nM for B16F10 and A549 cells, respectively) was higher than that of free DOX (44 ± 4 nM for B16F10 cells and 370 ± 70 nM for A549 cells). Although the IC50 of DOX-NG (180 ± 30 nM for B16F10 cells and 1700 ± 200 nM for A549 cells) was higher than that of free DOX, the value is lower than that of DOX-MA (370 ± 30 nM for B16F10 cells and 2400 ± 300 nM for A549 cells). PEG-DOX-NG (IC50 of 200

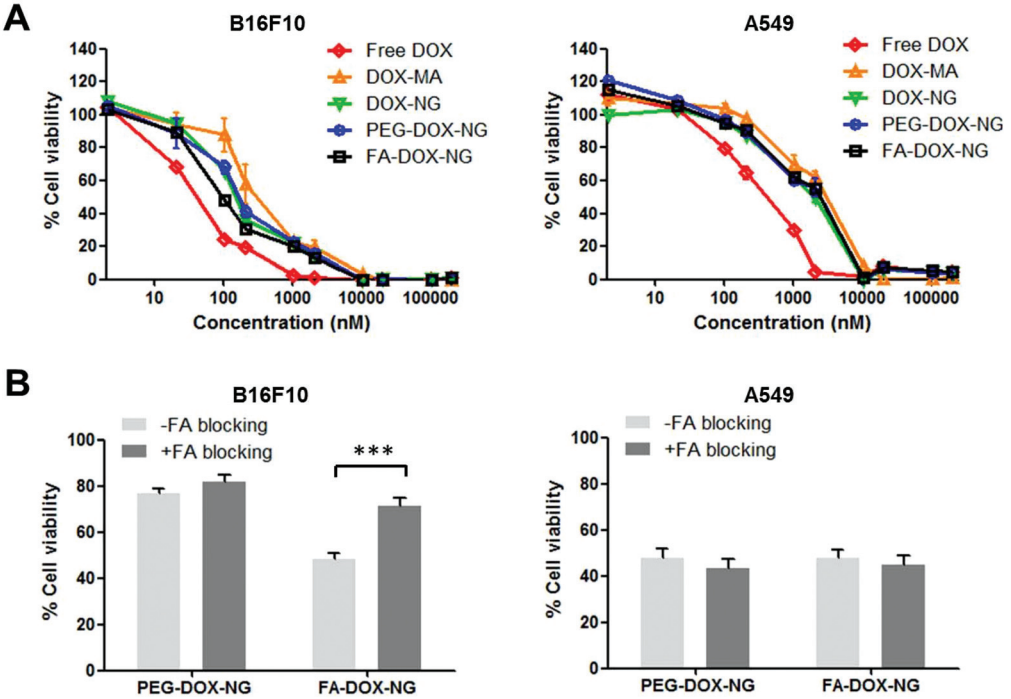

Fig. 8 (A) Viability of B16F10 and A549 cells after incubation with free DOX, DOX-MA and DOX loaded nanogel formulations for 72 h at 37 °C (n = 3). (B) Viability of B16F10 and A549 cells after incubation with PEG-DOX-NG and FA-DOX-NG (at IC50 of FA-DOX-NG, 100 nM for B16F10 cells and 1900 nM for A549 cells) with/without folic acid (1 mM) for 72 h at 37 °C (n = 10, ***p < 0.001).

± 30 and 1800 ± 400 for B16F10 and A549 cells, respectively) showed slightly less cytotoxicity than the DOX-NG. For B16F10, which is a folate receptor positive cell line, FA-DOX-NG showed higher cytotoxicity than PEG-DOX-NG (IC50 of 120 ± 20 nM for FA-DOX-NG and 200 ± 27 nM for PEG-DOX-NG). On the other hand, for A549 which is a folate receptor negative cell line, FA-DOX-NG and PEG-DOX-NG had similar IC50 values (around 1800 nM).

It is well known that free DOX can spontaneously permeate through both the cell and nuclear membrane, accumulate in the cell nucleus which leads to cell apoptosis.[59] The uptake of DOX-MA by cells is much lower than free DOX as shown in section 3.6.1. But even if DOX-MA can pass through the membrane by passive diffusion it ends up in the cytoplasm, where it is very slowly converted into DOX. Therefore the cytotoxicity of DOX-MA is lowest among all formulations on both cell lines. DOX-NG showed a much higher cytotoxicity than DOX-MA (Fig. 8A and Table S2†) which can be ascribed to endosomal uptake of the nanogels and subsequent DOX release. PEG-DOX-NG displayed less cytotoxic effects on both cells than DOX-NG due to the less cellular uptake (Fig. 5). FA-DOX-NG showed a similar IC50 as PEG-DOX-NG on folate receptor negative (A549) cells, whereas higher cytotoxicity than PEG-DOX-NG. Considering good cytocompatibility of blank nanogels[24] and PEG[64] as well as limited amount of folic acid, no difference in cytotoxicity of the distinct nanogel formulations (without drug) is expected. Together with the cellular uptake and subcellular distribution studies, cytotoxicity study suggests that FA decorated nanogels can be internalized by receptor-mediated endocytosis, increase intracellular drug concentration and in turn enhance the cytotoxicity against folate receptor positive cancer cells.

3.6.5 Competitive inhibition. To investigate whether the FA-decorated nanogels were indeed taken up by the FA receptor, FA was added to the culture medium of B16F10 (folate receptor positive) cells and A549 (folate receptor negative) cells. Fig. 8B shows that incubation of A549 cells with either PEG-DOX-NG or FA-DOX-NG resulted in the same cytotoxic values, both in the absence and presence of free FA in the medium. On the other hand, incubation of B16F10 cells with FA-DOX-NG resulted in a substantially higher cytotoxicity at the same DOX concentration (100 nM) than PEG-DOX-NG (cell viability 76.8 ± 1.9% for PEG-DOX-NG and 48.5 ± 2.6% for FA-DOX-NG). The cell viability upon incubation with FA-DOX-NG in the presence of FA (71.2 ± 3.8%) significantly increased (p < 0.001) and reached almost the same level as viability of cells incubated with PEG-DOX-NG (81.6 ± 3.0%). This demonstrates that free FA can inhibit the cellular uptake of FA-modified nanogels, which again points to receptor mediated uptake of these nanoparticles in the absence of FA in the medium.

3.7 Uptake and efficacy in DOX-sensitive and DOX-resistant 4T1 cells

3.7.1 Cellular uptake of DOX, DOX-MA and DOX-loaded nanogels by DOX-sensitive and -resistant 4T1 cells. First,

increased levels of MDR1 mRNA and Pgp protein expression were confirmed by means of RT-PCR and immunofluorescence intensity, respectively (Fig. S8†). Then, DOX-resistant 4T1 cells which overexpress FR were incubated with FA-DOX-NG to investigate whether this formulation can overcome MDR. Fig. 9A (upper panel) shows the cellular uptake of different DOX formulations by DOX-sensitive 4T1 cells. Strong fluorescence signal of DOX was observed when DOX-sensitive 4T1 cells were incubated with free DOX, while a low signal was found when the sensitive cells were incubated with DOX-MA. After DOX-MA was loaded into nanogels to form DOX-NG, a substantially increased signal of DOX in the sensitive cells was observed. The fluorescence intensity of DOX for sensitive cells incubated with PEG-DOX-NG was slightly less than that of cells exposed to DOX-NG.

Fig. 9A (lower panel) shows that the fluorescence intensity of DOX in resistant cells after incubation with the different formulations was less than that observed in sensitive cells. A DOX signal was hardly detectable in the resistant cells after incubation with either free DOX or DOX-MA. The figures also show that the uptake of DOX-MA by resistant cells was improved by DOX-NG. However, the uptake of PEGylated nanogels (PEG-DOX-NG) was decreased. It can be explained by the reduced nanogel–cell interactions because of PEG interference.[65] Importantly, the resistant cells incubated with FA-DOX-NG displayed about 3 times higher DOX uptake than free DOX (Fig. 9B).

3.7.2 Cytotoxicity of DOX-loaded nanogels in DOX-sensitive and -resistant 4T1 cells. An XTT assay was performed to evaluate the efficacy of free DOX, DOX-MA and DOX loaded nanogel formulations on the DOX-sensitive and -resistant 4T1 cells (Fig. 9 and Table S3†). In the sensitive cells, free DOX showed a higher cytotoxicity than DOX-MA (IC50 1000 ± 200 nM for free DOX and 4500 ± 600 nM for DOX-MA). DOX-NG (IC50 1100 ± 100 nM) was slightly less toxic than free DOX, and nanogels showed less effect after PEGylation (IC50 1500 ± 300 nM for PEG-DOX-NG). However, the IC50 decreased after decoration of the nanogels with FA (FA-DOX-NGs, IC50 900 ± 200 nM), indicating the formulation becomes more cytotoxic.

Table S3† shows that free DOX, DOX-MA and the different nanogel formulations were less cytotoxic (had a higher IC50 value) towards DOX resistant 4T1 cells as compared to sensitive cells, as reported in many other studies.[66]

The efficacies of the different formulations in the resistant and sensitive cells were compared by the so-called resistance index (RI, defined as section 2.5.3, eqn (5)) (Table S3†). The RI of DOX-NG is similar to that of free DOX (11.2 ± 1.6 *vs.* 13.4 ±

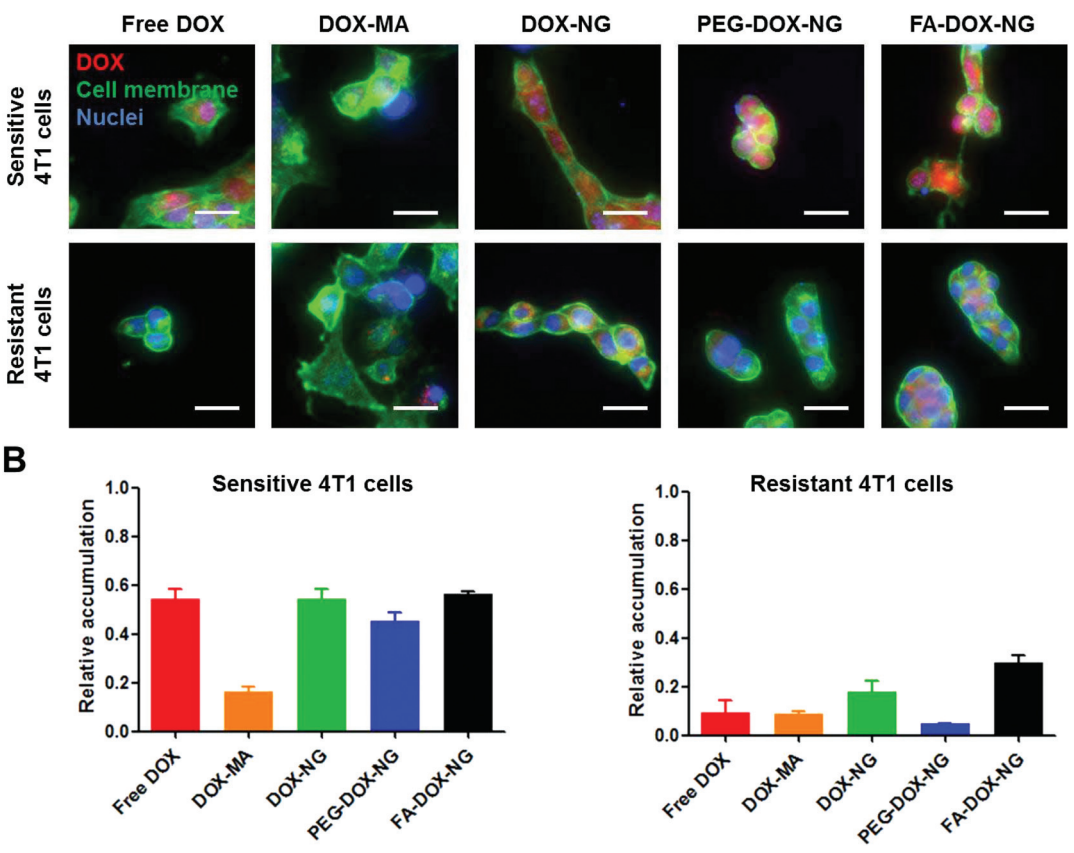

Fig. 9 (A) Fluorescence microscopy images of sensitive and resistant 4T1 cells incubated with free DOX, DOX-MA and nanogel formulations (10 000 nM equivalent DOX) for 24 h at 37 °C; nuclei are stained in blue with DAPI, cell membranes are stained in green with WGA and DOX is presented in red. (B) Relative accumulation of different DOX formulations in the cells by measuring the fluorescence intensity of DOX ($\lambda_{ex.}$ 488 nm, $\lambda_{em.}$ 600 nm). Bars, 50 μm.

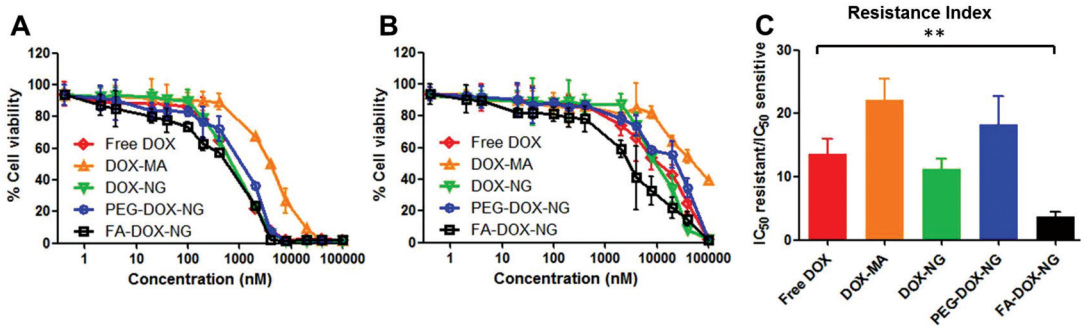

Fig. 10 Viability of DOX (A) sensitive and (B) resistant 4T1 cells after incubation with free DOX, DOX-MA and nanogel formulations for 72 h at 37 °C. (C) Resistance index of free DOX, DOX-MA and nanogel formulations (n = 3, $^{**}p < 0.01$).

2.4) whereas the RI of PEG-DOX-NG (18.3 ± 4.5) is even higher than that of free DOX and DOX-NG. Importantly, the RI of the active targeted formulation FA-DOX-NG is 3.7 ± 0.8, which is significantly lower (~4-fold, $p < 0.01$) than that of free DOX.

No significant difference in RI was found between free DOX and DOX-NG, unlike the common opinion that nanomedicines can bypass the drug efflux pumps on the surface of resistant cell membranes resulting in significant better anticancer efficacy.[67–69] A similar conclusion was also obtained by Kunjachan *et al.*[70] who tested other nanomedicines for different types of MDR and concluded that the ability of nanomedicines to overcome MDR cannot be overestimated and generalized. In contrast, FA-DOX-NG showed much higher cytotoxicity on the resistant cells and its RI was significantly lower than other formulations. These results demonstrate that FA-decorated nanogels can bypass the MDR pump, be internalized into cells by receptor mediated endocytosis and release the payloads to cause cytotoxicity (Fig. 10).

4 Conclusions

In the present study, we combined pH controlled drug release and an active targeting strategy in one formulation to overcome MDR. The nanocarriers showed complete drug release within 24 h at mild acidic pH (pH 5). The nanogels are able to be internalized by receptor-mediated endocytosis and increase cellular uptake and cytotoxicity against folate receptor positive cells. The active targeting was further confirmed by competitive inhibition by an excess folic acid. The system displays superior antitumor effect on folate receptor upregulated drug resistant breast cancer cells. This paper shows that nanogels with pH sensitive drug release and active targeting hold significant potential to be an effective chemotherapeutics with enhanced toxicity against folate receptor overexpressing cancer cells and overcoming multidrug resistance.

Acknowledgements

This work was supported by the China Scholarship Council, the German Academic Exchange Service (DAAD) (Grant No.: 57048249), and the Ministry of Education, Youth and Sports of CR within the National Sustainability Program I, Project POLYMAT LO1507.

References

1 B. B. S. Cerqueira, A. Lasham, A. N. Shelling and R. Al-Kassas, *Eur. J. Pharm. Biopharm.*, 2015, **97**(Part A), 140–151.
2 J. M. Huitink and W. H. L. Teoh, *Best Pract. Res., Clin. Anaesthesiol.*, 2013, **27**, 481–492.
3 Y. H. Bae and K. Park, *J. Controlled Release*, 2011, **153**, 198–205.
4 Y. Liu, G. Wan, H. Guo, Y. Liu, P. Zhou, H. Wang, D. Wang, S. Zhang, Y. Wang and N. Zhang, *Nano Res.*, 2017, **10**, 834–855.
5 M. M. Gottesman, *Annu. Rev. Med.*, 2002, **53**, 615–627.
6 C. Holohan, S. Van Schaeybroeck, D. B. Longley and P. G. Johnston, *Nat. Rev. Cancer*, 2013, **13**, 714–726.
7 O. Tezcan, T. Ojha, G. Storm, F. Kiessling and T. Lammers, *Expert Opin. Drug Delivery*, 2016, **13**, 1199–1202.
8 S. Kunjachan, B. Rychlik, G. Storm, F. Kiessling and T. Lammers, *Adv. Drug Delivery Rev.*, 2013, **65**, 1852–1865.
9 L. Mei, G. Zhu, L. Qiu, C. Wu, H. Chen, H. Liang, S. Cansiz, Y. Lv, X. Zhang and W. Tan, *Nano Res.*, 2015, **8**, 3447–3460.
10 G. Sahay, D. Y. Alakhova and A. V. Kabanov, *J. Controlled Release*, 2010, **145**, 182–195.
11 Y.-C. Wang, F. Wang, T.-M. Sun and J. Wang, *Bioconjugate Chem.*, 2011, **22**, 1939–1945.
12 Y. Zhu, J. Zhang, F. Meng, C. Deng, R. Cheng, J. Feijen and Z. Zhong, *J. Controlled Release*, 2016, **233**, 29–38.
13 R. T. Chacko, J. Ventura, J. Zhuang and S. Thayumanavan, *Adv. Drug Delivery Rev.*, 2012, **64**, 836–851.
14 D. Li, F. Sun, M. Bourajjaj, Y. Chen, E. H. Pieters, J. Chen, J. B. van den Dikkenberg, B. Lou, M. G. M. Camps, F. Ossendorp, W. E. Hennink, T. Vermonden and C. F. van Nostrum, *Nanoscale*, 2016, **8**, 19592–19604.
15 Z. Cao and U. Ziener, *Nanoscale*, 2013, **5**, 10093–10107.
16 J. K. Oh, R. Drumright, D. J. Siegwart and K. Matyjaszewski, *Prog. Polym. Sci.*, 2008, **33**, 448–477.
17 Y. Ma, Y. Ge and L. Li, *Mater. Sci. Eng., C*, 2017, **71**, 1281–1292.

18 J. Zhang, R. Chen, X. Fang, F. Chen, Y. Wang and M. Chen, *Nano Res.*, 2015, **8**, 201–218.
19 D. Peer, J. M. Karp, S. Hong, O. C. Farokhzad, R. Margalit and R. Langer, *Nat. Nanotechnol.*, 2007, **2**, 751–760.
20 G. Morral-Ruíz, P. Melgar-Lesmes, A. López-Vicente, C. Solans and M. J. García-Celma, *Nano Res.*, 2015, **8**, 1729–1745.
21 X. Yang, A. K. lyer, A. Singh, E. Choy, F. J. Hornicek, M. M. Amiji and Z. Duan, *Sci. Rep.*, 2015, **5**, 8509.
22 X.-B. Xiong and A. Lavasanifar, *ACS Nano*, 2011, **5**, 5202–5213.
23 Y. Lu and P. S. Low, *Adv. Drug Delivery Rev.*, 2002, **54**, 675–693.
24 Y. Chen, M. J. van Steenbergen, D. Li, J. B. van de Dikkenberg, T. Lammers, C. F. van Nostrum, J. M. Metselaar and W. E. Hennink, *Macromol. Biosci.*, 2016, **16**, 1122–1137.
25 W. N. E. van Dijk-Wolthuls, S. K. Y. Tsang, J. J. Kettenes-van den Bosch and W. E. Hennink, *Polymer*, 1997, **38**, 6235–6242.
26 J. A. Cadée, M. De Kerf, C. J. De Groot, W. Den Otter and W. E. Hennink, *Polymer*, 1999, **40**, 6877–6881.
27 T. Etrych, M. Jelínková, B. Říhová and K. Ulbrich, *J. Controlled Release*, 2001, **73**, 89–102.
28 M. F. Ebbesen, D. H. Schaffert, M. L. Crowley, D. Oupický and K. A. Howard, *J. Polym. Sci., Part A: Polym. Chem.*, 2013, **51**, 5091–5099.
29 M. Talelli, K. Morita, C. J. F. Rijcken, R. W. M. Aben, T. Lammers, H. W. Scheeren, C. F. van Nostrum, G. Storm and W. E. Hennink, *Bioconjugate Chem.*, 2011, **22**, 2519–2530.
30 L. Novo, E. Mastrobattista, C. F. van Nostrum and W. E. Hennink, *Bioconjugate Chem.*, 2014, **25**, 802–812.
31 J. H. van Steenis, E. M. van Maarseveen, F. J. Verbaan, R. Verrijk, D. J. A. Crommelin, G. Storm and W. E. Hennink, *J. Controlled Release*, 2003, **87**, 167–176.
32 J. M. Benns, A. Maheshwari, D. Y. Furgeson, R. I. Mahato and S. W. Kim, *J. Drug Targeting*, 2001, **9**, 123–139.
33 K. Raemdonck, B. Naeye, K. Buyens, R. E. Vandenbroucke, A. Høgset, J. Demeester and S. C. De Smedt, *Adv. Funct. Mater.*, 2009, **19**, 1406–1415.
34 E. Oude Blenke, G. Klaasse, H. Merten, A. Plückthun, E. Mastrobattista and N. I. Martin, *J. Controlled Release*, 2015, **202**, 14–20.
35 J.-F. Lutz, *Angew. Chem., Int. Ed.*, 2008, **47**, 2182–2184.
36 Y. Jiang, J. Chen, C. Deng, E. J. Suuronen and Z. Zhong, *Biomaterials*, 2014, **35**, 4969–4985.
37 R. J. H. Stenekes and W. E. Hennink, *Polymer*, 2000, **41**, 5563–5569.
38 M. Talelli, M. Iman, A. K. Varkouhi, C. J. F. Rijcken, R. M. Schiffelers, T. Etrych, K. Ulbrich, C. F. van Nostrum, T. Lammers, G. Storm and W. E. Hennink, *Biomaterials*, 2010, **31**, 7797–7804.
39 T. Etrych, T. Mrkvan, P. Chytil, Č. Koňák, B. Říhová and K. Ulbrich, *J. Appl. Polym. Sci.*, 2008, **109**, 3050–3061.
40 X.-L. Hu, H.-Y. Jin, X.-P. He, T. D. James, G.-R. Chen and Y.-T. Long, *ACS Appl. Mater. Interfaces*, 2015, **7**, 1874–1878.
41 K. J. Livak and T. D. Schmittgen, *Methods*, 2001, **25**, 402–408.
42 K. W. Dunn, M. M. Kamocka and J. H. McDonald, *Am. J. Physiol.: Cell Physiol.*, 2011, **300**, C723–C742.
43 J. Adler and I. Parmryd, *Cytometry, Part A*, 2010, **77**, 733–742.
44 S.-L. Kim, H.-J. Jeong, E.-M. Kim, C.-M. Lee, T.-H. Kwon and M.-H. Sohn, *J. Korean Med. Sci.*, 2007, **22**, 405–411.
45 A. F. Trindade, R. F. M. Frade, E. M. S. Macoas, C. Graca, C. A. B. Rodrigues, J. M. G. Martinho and C. A. M. Afonso, *Org. Biomol. Chem.*, 2014, **12**, 3181–3190.
46 L. Bomgaars, S. Gunawardena, S. E. Kelley and A. Ramu, *Cancer Chemother. Pharmacol.*, 1997, **40**, 506–512.
47 S. H. Hilal, S. W. Karickhoff, L. A. Carreira and B. P. Shrestha, *QSAR Comb. Sci.*, 2003, **22**, 917–925.
48 D. Neradovic, M. J. van Steenbergen, L. Vansteelant, Y. J. Meijer, C. F. van Nostrum and W. E. Hennink, *Macromolecules*, 2003, **36**, 7491–7498.
49 H. C. Kolb and K. B. Sharpless, *Drug Discovery Today*, 2003, **8**, 1128–1137.
50 E. H. P. Leunissen, M. H. L. Meuleners, J. M. M. Verkade, J. Dommerholt, J. G. J. Hoenderop and F. L. van Delft, *ChemBioChem*, 2014, **15**, 1446–1451.
51 G. Zhang, Z. Yang, W. Lu, R. Zhang, Q. Huang, M. Tian, L. Li, D. Liang and C. Li, *Biomaterials*, 2009, **30**, 1928–1936.
52 T. L. Moore, L. Rodriguez-Lorenzo, V. Hirsch, S. Balog, D. Urban, C. Jud, B. Rothen-Rutishauser, M. Lattuada and A. Petri-Fink, *Chem. Soc. Rev.*, 2015, **44**, 6287–6305.
53 A. A. Lohade, R. R. Jain, K. Iyer, S. K. Roy, H. H. Shimpi, Y. Pawar, M. G. R. Rajan and M. D. Menon, *AAPS PharmSciTech*, 2016, **17**, 1298–1311.
54 E. S. Krystofiak, V. Z. Matson, D. A. Steeber and J. A. Oliver, *J. Nanomater.*, 2012, **2012**, 9.
55 S. Jain, G. Spandana, A. K. Agrawal, V. Kushwah and K. Thanki, *Mol. Pharm.*, 2015, **12**, 3871–3884.
56 S. Mishra, P. Webster and M. E. Davis, *Eur. J. Cell Biol.*, 2004, **83**, 97–111.
57 F. Shen, S. Chu, A. K. Bence, B. Bailey, X. Xue, P. A. Erickson, M. H. Montrose, W. T. Beck and L. C. Erickson, *J. Pharmacol. Exp. Ther.*, 2008, **324**, 95–102.
58 S. K. Soininen, K.-S. Vellonen, A. T. Heikkinen, S. Auriola, V.-P. Ranta, A. Urtti and M. Ruponen, *Mol. Pharm.*, 2016, **13**, 1358–1365.
59 O. Hovorka, M. Šťastný, T. Etrych, V. Šubr, J. Strohalm, K. Ulbrich and B. Říhová, *J. Controlled Release*, 2002, **80**, 101–117.
60 S. K. Soininen, P. Lehtolainen-Dalkilic, T. Karppinen, T. Puustinen, G. Dragneva, M. U. Kaikkonen, M. Jauhiainen, B. Allart, D. L. Selwood, T. Wirth, H. P. Lesch, A.-M. Määttä, J. Mönkkönen, S. Ylä-Herttuala and M. Ruponen, *Eur. J. Pharm. Sci.*, 2012, **47**, 848–856.
61 Z. Farhane, F. Bonnier and H. J. Byrne, *Anal. Bioanal. Chem.*, 2017, **409**, 1333–1346.
62 S. Zhang, H. Gao and G. Bao, *ACS Nano*, 2015, **9**, 8655–8671.
63 M. Talelli, S. Oliveira, C. J. F. Rijcken, E. H. E. Pieters, T. Etrych, K. Ulbrich, R. C. F. van Nostrum, G. Storm,

W. E. Hennink and T. Lammers, *Biomaterials*, 2013, **34**, 1255–1260.
64 G. Liu, Y. Li, L. Yang, Y. Wei, X. Wang, Z. Wang and L. Tao, *RSC Adv.*, 2017, **7**, 18252–18259.
65 Z. Amoozgar and Y. Yeo, *Wiley Interdiscip. Rev.: Nanomed. Nanobiotechnol.*, 2012, **4**, 219–233.
66 F. M. Kievit, F. Y. Wang, C. Fang, H. Mok, K. Wang, J. R. Silber, R. G. Ellenbogen and M. Zhang, *J. Controlled Release*, 2011, **152**, 76–83.
67 M. Kamimura, T. Furukawa, S.-i. Akiyama and Y. Nagasaki, *Biomater. Sci.*, 2013, **1**, 361–367.
68 Y. Yuan, T. Cai, X. Xia, R. Zhang, P. Chiba and Y. Cai, *Drug Delivery*, 2016, 1–8, DOI: 10.1080/10717544.2016.1178825.
69 J. Shen, Q. He, Y. Gao, J. Shi and Y. Li, *Nanoscale*, 2011, **3**, 4314–4322.
70 S. Kunjachan, A. Błauż, D. Möckel, B. Theek, F. Kiessling, T. Etrych, K. Ulbrich, L. v. Bloois, G. Storm, G. Bartosz, B. Rychlik and T. Lammers, *Eur. J. Pharm. Sci.*, 2012, **45**, 421–428.